Available online at www.sciencedirect.com

SciVerse ScienceDirect

Ceramics International 38 (2012) 5613–5620

CERAMICS INTERNATIONAL

www.elsevier.com/locate/ceramint

Dispersant-assisted low frequency electrophoretically deposited TiO_2 nanoparticles in non-aqueous suspensions for gas sensing applications

Javad Esmaeilzadeh [a], Sasan Ghashghaie [a], Babak Raissi [a,*], Ehsan Marzbanrad [a], Cyrus Zamani [b], Reza Riahifar [a]

[a] Department of Ceramic, Materials and Energy Research Center, Tehran 14155-4777, Iran
[b] XaRMAE/IN2UB, Department of Electronica, Universitat de Barcelona, 08028 Barcelona, Spain

Received 12 January 2012; received in revised form 31 March 2012; accepted 2 April 2012
Available online 9 April 2012

Abstract

The effect of dispersant on deposition mechanism of TiO_2 nanoparticles at 1 Hz under non-uniform AC fields was investigated. It was found that by adding Dolapix to suspension, deposition pattern is drastically changed enabling particles to enter the gap leaving the electrodes intact. Using low frequency AC electrophoretic deposition technique in the presence of dispersant, we succeeded in fabricating gas sensor in less than 2 min. Gas sensing measurements were performed in the temperature range of 450–550 °C. The results explained that the sensor has good stability in time and repeatability performance toward high response. The maximum sensitivity of about 180 for the TiO_2 nanoparticles sensor is observed with 47 ppm NO_2 gas and the response and recovery times is about 60–150 s. The optimum temperature of the gas sensor was obtained in 450 °C where sensor showed a linear trend up to 50 ppm of NO_2 gas. This sensing behavior in un-doped TiO_2 as NO_2 sensor can be mainly ascribed to the porous structure of the sensing film and its good contacts to the substrate and electrode assembly.

Keywords: TiO_2 nanoparticles; AC electrophoretic deposition; Dispersant; NO_2 gas sensing

1. Introduction

Detection of toxic and pollutant gases generated by factories and cars such as NO_x, CO, H_2 and CH_4 is a considerable subject for monitoring and controlling industrial processes and environmental applications [1]. Semiconductor gas sensors based on metal oxides in comparison to other chemical gas sensors are more attractive due to their high sensitivity to toxic gas and less price [2]. Among the wide variety of metal oxides such as ZnO, In_2O_3, SnO_2 and WO_3, TiO_2 is a good choice for the fabrication of high temperature gas sensors. TiO_2 is an n-type metal oxide semiconductor with a band gap of about 3.2 eV [3]. It is chemically and thermally stable at high temperatures [4].

The origin of gas sensing is based on the interaction of sensing material with gas molecule and changes of electrical resistivity of material due to chemisorptions of gas molecules on the sensing material surface [5]. Therefore, according to this sensing mechanism, the surface of the material would play a key role. In this regard, the different sensor fabrication methods are used to achieve higher surface area and consequently gas sensors with better performance.

Among the wide variety of sensor fabrication methods, low frequency AC electrophoretic deposition (LFACEPD) [6–9] is a method with high potential for controlled deposition of nanomaterials and meanwhile a simple reproducible way for the manipulation of ceramic nanoparticles. While in DC non-uniform electric fields particles move along the electric field lines in one direction towards the opposite electrode, AC fields offer a chance for the reversal of particles direction in each cycle [10].

While at high frequencies the dielectrophoresis force caused by the electric field gradient is responsible for particles movement, at low frequencies oscillatory columbic force is the dominant force acting on the charged particles making them migrate along the electric field lines in each cycle [11]. However, at low frequencies such as 1 Hz, contrary to what is expected, the net movement of particles is not zero and they

* Corresponding author.
E-mail address: babakraissi@yahoo.com (B. Raissi).

0272-8842/$36.00
http://dx.doi.org/10.1016/j.ceramint.2012.04.002

have been observed to deposit on both electrodes and finally filling the inter-electrode gap. Hence, the deposition rate as well as the obtained layer microstructure is expected to be highly dependent on the ability of the medium to bear charge on the surface of the particles.

Dolapix CE 64 is an electrostric polyelectrolyte dispersant which has been used to successfully disperse the ceramic particles such as alumina [12], zirconia [13], silicon nitride suspensions [14] and cordierite-based glass ceramics [15] in aqueous media. In this study, we investigated the effect of Dolapix CE 64 addition to an organic media (acetone) on the deposition behavior of TiO_2 nanoparticles at 1 Hz. Subsequently, using the LFACEPD method a TiO_2 gas sensor was fabricated in a short time interval and its response in the presence of NO_2 gas was studied.

2. Experimental

2.1. Materials and characterization

The TiO_2 nanopowder which was used in the present research was P25 purchased from Deggusa Company. Powder morphology was investigated by SEM (SEM, Cambridge-S360) and its crystal structure was determined by XRD (PHILIPS-PW3710, Bragg–Brentano geometry, Cu $K_{\alpha 1}$ X-ray source, wavelength 1.5406 Å, 20–85°). This powder was used for electric-field assisted deposition after preparation of a stable suspension which is suitable for ACEPD. A commercial polyelectrolyte Dolapix CE 64 purchased from Zschimmer and Schwarz GmbH Co., Germany, was used as dispersant. For this purpose, 12 g/l solution of Dolapix CE 64 in distilled water was prepared. A 0.3 g/l TiO_2 suspension in pure acetone (Merck Art. #12) was prepared and three drops of the diluted Dolapix solution was added to the suspension. At the next step, the suspension was ultrasonicated for 15 min to break up the agglomerates. For comparison, a dispersant free TiO_2 suspension was prepared using the same procedure. Both suspensions were characterized by measuring the Zeta potential of TiO_2 nanoparticles by Malvern Zetasizer (3000 HAS). Also, the conductivity of the prepared suspensions was measured using a WTW-inolab conductivity meter.

2.2. AC electrophoretic deposition

Deposition of TiO_2 nanoparticles was done using an electrophoretic setup consisting of a function generator (RIGOL DG 1022) to generate sinusoidal AC electric fields. The peak-to-peak voltage of the applied sinusoid wave for all experiments was chosen to be 5 V. A voltage amplifier (hp 6826 A) was employed to increase the output voltage to 30 V. Deposition of TiO_2 nanoparticles from the prepared suspension was performed at 1 Hz on coplanar gold electrodes. The coplanar gold electrodes were fabricated on a borosilicate glass using commercial gold paste (Degussa Inc., GZ117). The gold layer was dried and stabilized by firing at 610 °C for 1 h. Then, using laser beam, a notch was created on the gold layer separating it into two planar parallel electrodes with gap width of about 180 μm.

Each ACEPD experiment was performed twice, one time from a dispersant-free suspension of TiO_2 and the next time using the suspension prepared through the addition of Dolapix as the dispersing agent. Optical microscopy (Olympus DP72, Tokyo, Japan) was employed to study the deposition pattern at different conditions.

2.3. Sensor fabrication and sensor response measurement

Sensor fabrication was performed on interdigitated platinum electrodes from a 0.3 g/l TiO_2 suspension containing three drops of Dolapix as dispersant. Deposition of TiO_2 nanoparticles from the prepared suspension was accomplished at 1 Hz and applied voltage of 30 V. The interdigitated platinum electrodes were designed on an alumina sheet equipped with a heater on the backside in order to reach the desired working temperature. Response of the sensor toward various concentration of NO_2 gas at different temperatures was measured and recorded in a fully automated dynamic gas sensor testing setup whose equivalent circuit is schematically illustrated by Fig. 1. The testing sensor (R_x) and sampling resistor (R_s = 1.62 MΩ) were in a series loop. Under a constant voltage source of 20 V, the voltage changes of the sampling resistor (R_s) reflects the resistivity change of the testing sensor. What is recorded by the gas sensing setup is the variable voltage that is inversely proportional to the resistance of the testing sensor. The sensor was stabilized by exposing to N_2 gas for 1 h before each sensing test. The target gas (NO_2) was diluted to reach pre-designed concentrations by mixing the gas with N_2 (base gas) using a digital flow controller. The gaseous mixture was then flown through the sensor chamber.

3. Results and discussion

3.1. AC electric field-assisted deposition at 1 Hz

Fig. 2 illustrates the XRD pattern corresponding to TiO_2 nanoparticles which is composed of a mixture of anatase (as a dominant phase) and rutile. The SEM image of particles shown in Fig. 3 reveals that the particles are below 100 nm in diameter and their morphology is spherical in shape. Suspension conductivity in the absence of dispersant was about 0.2 μS/cm and after the addition of dispersant was increased to 1.3 μS/cm. This is a direct result of the presence of ions of the dispersant in the suspension. The results of zeta potential analyses performed on prepared suspensions with/without dispersant obviously confirm that the presence of dispersant in the system will increase zeta potential value from 23.5 to 66.26 mV. Based on the chemical structure of Dolapix [13], it can be inferred that an electrostatic attraction between negatively charged groups of Dolapix and TiO_2 surface (positively charged) occurs and leads to more negative zeta potential values for TiO_2 nanoparticles in the systems containing Dolapix.

The zeta-potential results depicted by Fig. 4 as a function of Dolapix concentration clearly show that the surface charge of particles is increased as a result of the presence of dispersant within the medium. These results are in accordance with sedimentation tests (Fig. 5) for 10 and 24 h aging time durations

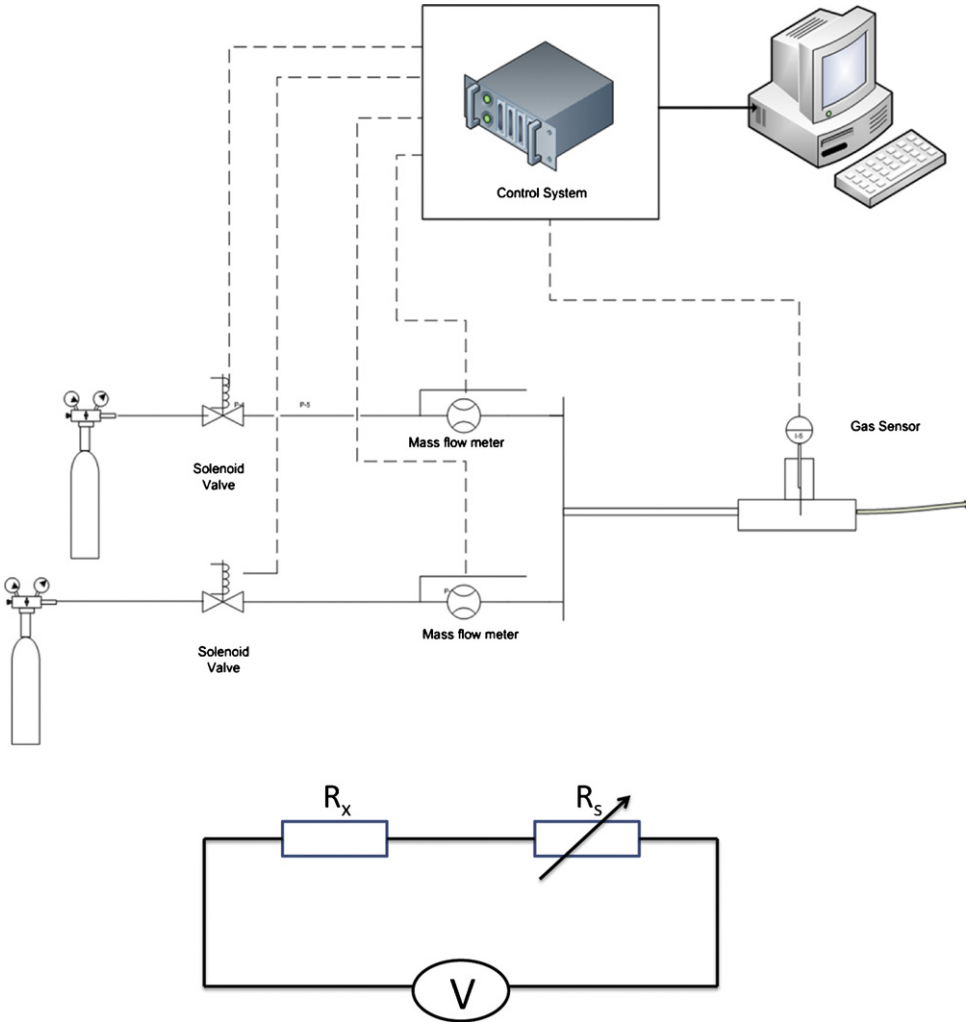

Fig. 1. Schematic of gas sensor setup with equivalent circuit.

where suspensions containing Dolapix were observed to preserve their stability for a longer period. It shows that the suspended particles in the colloidal suspension containing dispersant have acquired enough surface charge to repel the adjacent particles to avoid agglomeration. Hence, the suspension with Dolapix has lower settling rate.

According to Fig. 4, the maximum zeta potential is obtained for 3 drops of Dolapix based on which we expect to obtain the maximum deposition yield for the mentioned suspension. This fact is confirmed by the deposition yield variation as a function of Dolapix quantity depicted by Fig. 6, carried out on parallel planar gold electrodes at DC potential of 30 V. It clearly shows

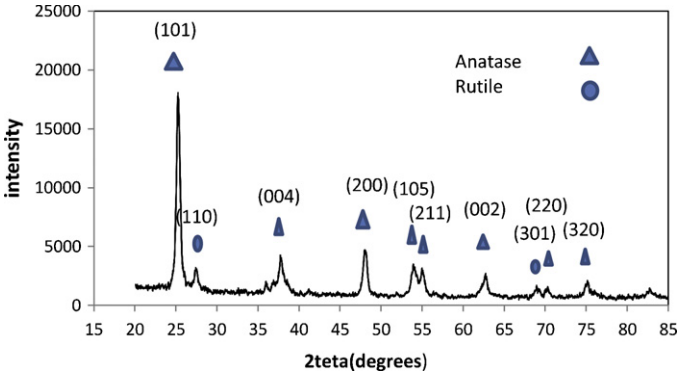

Fig. 2. XRD pattern of sensing material.

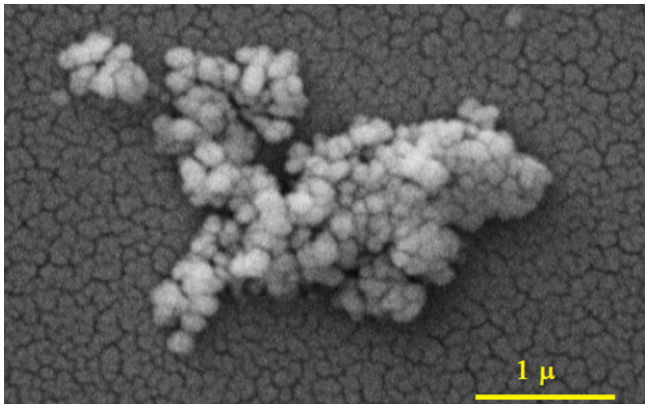

Fig. 3. Scanning electron micrograph of TiO_2 nanopowders.

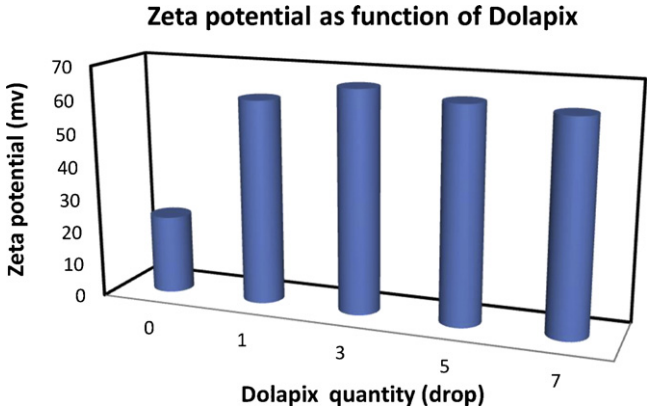

Fig. 4. Zeta potential variation as function of dispersant values (Dolapix CE64).

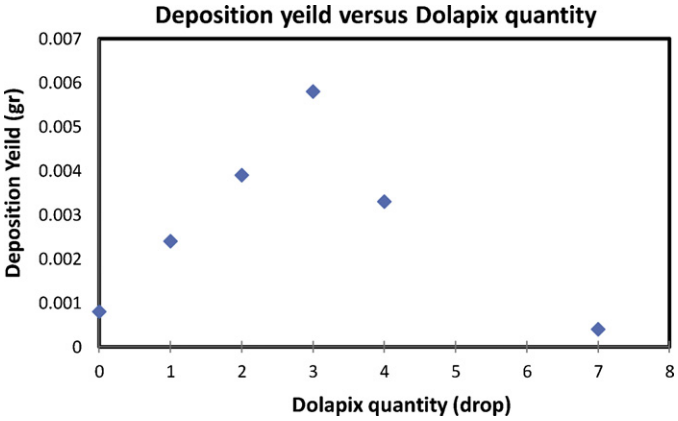

Fig. 6. Deposition yield variation versus Dolapix quantity.

that the highest deposited weight has been achieved for the suspension prepared by 3 drops of Dolapix.

Fig. 7 illustrates the deposition patterns of TiO_2 nanoparticles at 1 Hz from the suspension prepared without Dolapix (Fig. 7a) and the one prepared by adding 3 drops of the dispersant (Fig. 7b). As shown by optical microscopy images, a large fraction of TiO_2 particles have accumulated on both electrode surfaces and only a small fraction are observed to be trapped within the electrode gap. However, by adding Dolapix to the system, the deposition pattern was strongly changed where particles tended to massively fill the inter-electrode gap leaving the surface uncovered (Fig. 7b).

The above observations can be explained by the enhancement in mobility of particles due to increased surface charge density in presence of dispersant (as it is reflected in zeta-potential values). The electrophoretic mobility of the suspended particles is calculated by the Henry equation (1) as [16]:

$$\mu = \frac{2}{3}\frac{\varepsilon_0 \varepsilon_r \zeta}{\eta} f(kr) \quad (1)$$

where ε_0 is the permittivity of vacuum, ε_r is the relative permittivity of the solvent, η is the solvent viscosity, ζ is the zeta potential and $f(kr)$ is the Henry coefficient. In this equation, electrophoretic mobility of suspended particles depends linearly on the zeta potential and relative permittivity of the fluid and is inversely proportional to fluid viscosity.

While at 1 Hz the net movement of particles for symmetric wave in each cycle is expected to be zero, the ultimate deposition of nanoparticles on electrodes rejects this hypothesis. Two mechanisms may be considered for the deposition of suspended particles in the gap between electrodes. The first one is related to the non-steady state fluid flow. The origin of this flow is the electric field direction changes. When the electric field is turned on, in the first half-cycle, suspended particles and ions in the system start to move towards the electrode edges with opposite charge where the electric field strength is remarkably high. In the next half-cycle where direction of the electric field is reversed, the movement of particles and ions is changed. The occurrence of this alternating trend of ions/particles migration results in an unsteady state fluid flow near the electrode edges forcing the adjacent particles towards the inter-electrode gap [17]. The second factor responsible for particles deposition into the gap is the non-conductive substrate surface potential which was numerically simulated recently [18]. Based on this idea, the presence of this charged layer on

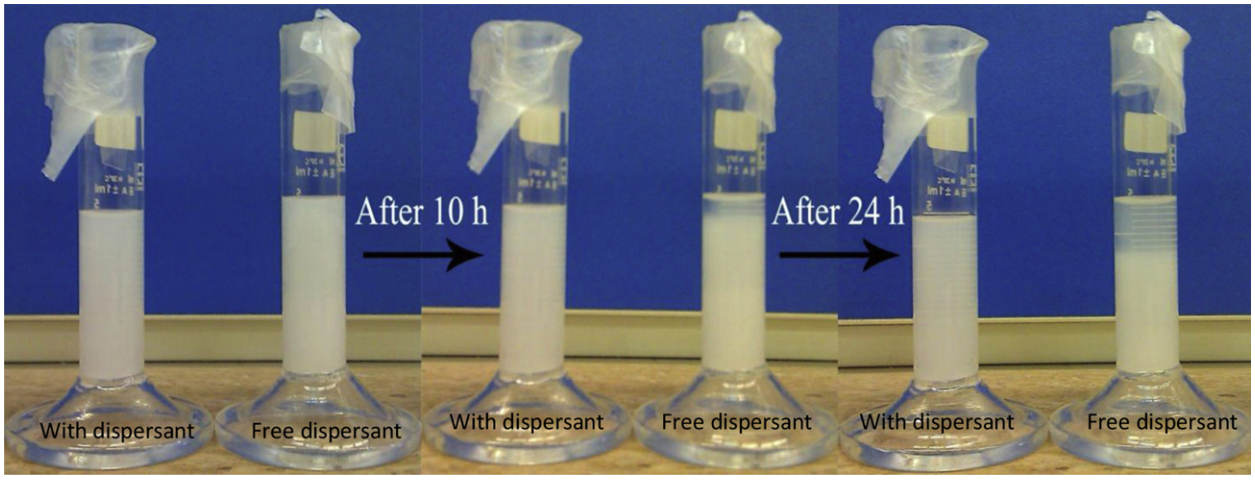

Fig. 5. Sedimentation test images in the presence and absence of Dolapix.

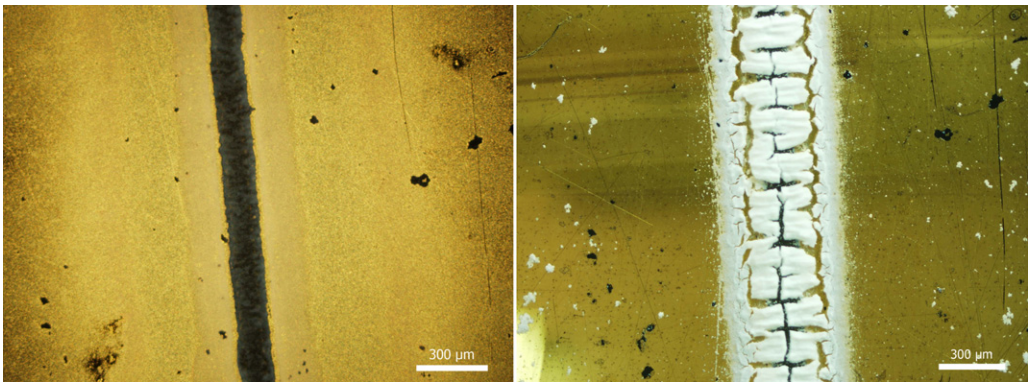

Fig. 7. Optical images of TiO_2 nanoparticles deposition pattern on gold co-planar electrodes: (a) in absence of Dolapix; (b) in presence of Dolapix.

the surface of the substrate will deviate the electric field lines from the electrode edges toward the gap. This will be able to conduct particles toward the gap letting them deposit there by columbic force.

The addition of Dolapix also improves the conductivity (the ionic strength) of the suspension. In this case, since the fluid flow is a result of ion migration toward the high electric field regions, it is expected that the fluid flow near the edges be enhanced at higher ionic strengths. Under such conditions, and in agreement with optical microscopy images, the possibility of fluid flow-assisted deposition of TiO_2 nanoparticles inside the gap can rise notably.

Considering the higher zeta potential of the suspension with Dolapix than suspension without dispersant and Eq. (1), it is expected that the suspended particles in the TiO_2/acetone system dispersed by Dolapix have high mobility and move toward high intensity electric field regions very fast. Because of high velocity of particles, they do not have enough time to select the most stable position for deposition which leads to the formation of severe cracks across the layer that is obviously presented by the optical microscope image of Fig. 7b. This phenomenon was attributed to the deposition rate of particles which hinders their assembly into a sufficiently packed structure and leads to the formation of cracks during the drying step [10]. In fact, at high deposition rates, resulted from high zeta potential, the possibility that the fluid is trapped within the layer is enhanced. This fluid tends to move upward the surface through the capillary effect during the drying step giving rise to substantial shrinkage across the film [19]. Thus, we used this technique for fast fabrication of TiO_2 gas sensors in about 1 min.

Generally, the results of obtained depositions from suspension with Dolapix in comparison with suspensions without dispersant can be explained by the above discussion. However, the disappearance of TiO_2 particles from the electrode surface is still a challenging result.

3.2. Sensor characterization and measurement

The optical image of deposition pattern of TiO_2 nanoparticles on interdigitated platinum electrode is depicted by Fig. 8. As it is seen, the sensing material has filled the gap between electrodes as well as the electrode surface. In fact, the isolated material left on the electrode surface has no contribution in the sensing phenomenon. Deposition of the particles on the surface of the electrodes which is different from coplanar gold electrodes can be attributed to the complexity of electric field lines in the interdigitated electrodes compared to co-planar gold electrodes as well as higher velocity of nanoparticles in suspension containing Dolapix. The sensing layer which is deposited on the sensor base plate is shown in SEM image (Fig. 9). These images present highly porous layer which can provide high-diffusivity path for target gas for maximized surface reactions.

For metal oxide semiconductor gas sensor, target gases diffuse into sensing layer through pores and react with sensing material. In this regard, the role of sensing film porosity on sensor response is more notable, especially for target gas with large molecular size. Sensor response to different NO_2 concentration operating in the temperature range of 450–550 °C is plotted in Fig. 10. The sensor response is calculated by (R_{gas}/R_{N2}) where R_{gas} and R_{N2} are the resistance of sensor exposed to base gas (N_2) and NO_2 as target gas, respectively. At each operating temperature, the sensor response followed a rising trend with increasing NO_2 concentration. Also, the high values of sensitivity obtained by TiO_2 nanoparticles based gas sensor loaded with un-doped material is about 180 which have

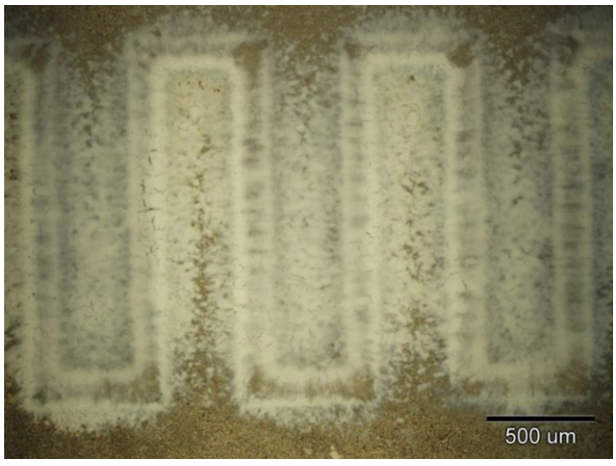

Fig. 8. Optical microscopy image of sensing interdigitated electrode.

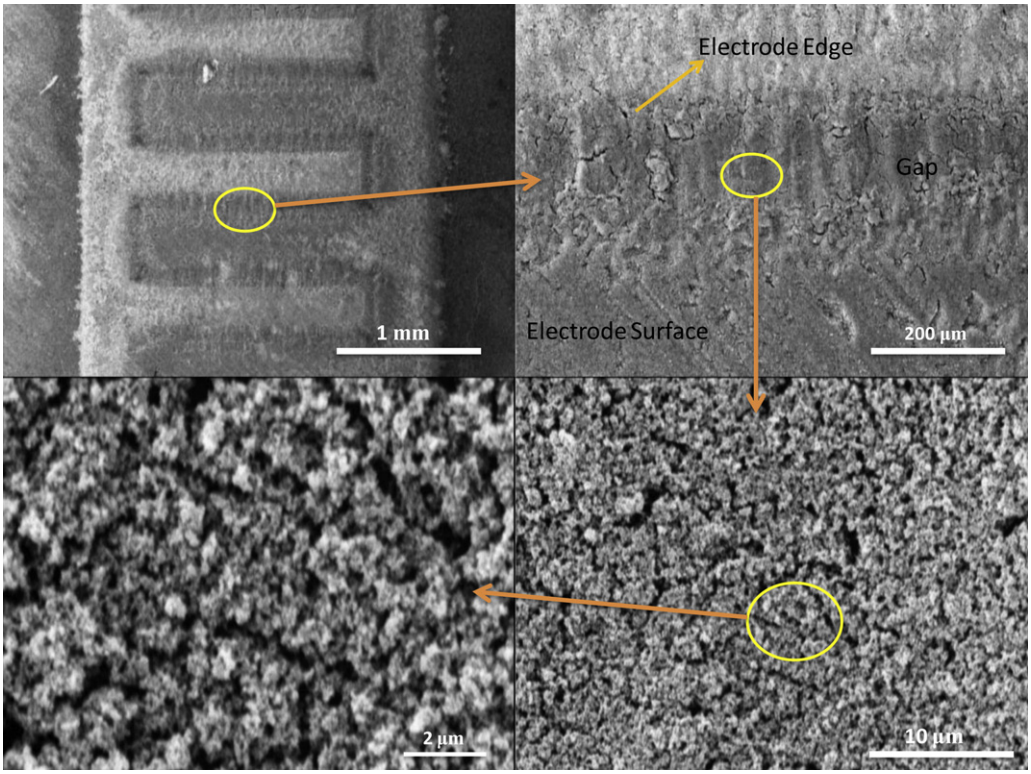

Fig. 9. SEM images of deposited sensing materials with different magnifications.

not been reported before this work since the TiO_2 in pure form has high resistance and consequently needs to be modified with the addition of dopants.

In comparison to other researches, Lin et al. [20] reported the maximum sensitivity of about 14 for the gas sensor based on TiO_2 nanocrystallites with 100 ppm NO_2 gas and the response time is about 1–3 min. Ruiz et al. [21] declared that the Cr-doped TiO_2 gas sensor has a response value of about 1.5 for 50 ppm of NO_2 gas at 500 °C. In another work, Carotta et al. [22] have evaluated thick films of nanostructured TiO_2 and niobium-doped TiO_2 prepared by screen-printing technology. They explained the electrical response for nanostructured TiO_2 gas sensor at 450 °C for 10 ppm of NO_2 gas to be about 2. The

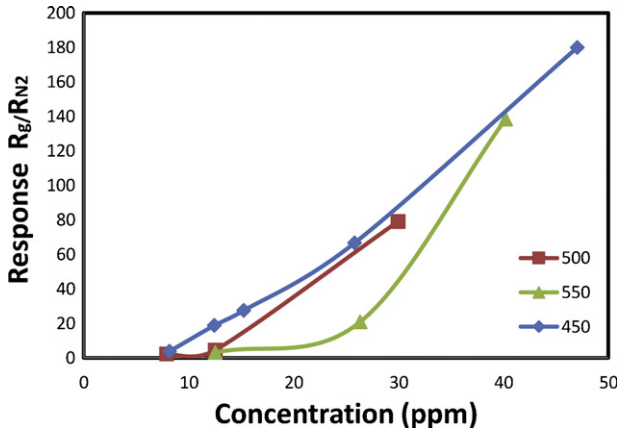

Fig. 10. Response values of sensor to different NO_2 concentrations at the temperature range of 450–550 °C.

optimum operating temperature giving the highest sensitivity has been determined about 450 °C for all tested sensors under different concentrations of NO_2 where sensor follows a linear trend up to 50 ppm of NO_2 gas. At elevated temperatures the desorption rate of gas species is too high in comparison with adsorption of gas targets so that the reversibility of the process is largely lost which will decrease the response value. The dynamic sensing plots showing the change in sensor resistance for various NO_2 concentrations operated at 450–550 °C are shown in Fig. 11. NO_2 gas molecules interact with the free electrons according to Eqs. (2) and (3) reducing the conductivity of the sensing layer.

$$NO_2 + e^- \rightarrow NO_2 \quad (2)$$

or

$$NO_2 + O_2^- + 2e^- \rightarrow NO_2^- + 2O^- \quad (3)$$

The sensor showed a stable baseline resistance, guaranteeing long term application in high temperatures. The sharp and non-regular increase in the sensor resistance in the *R* curves as shown in Fig. 11 reflects the overshooting in the gas concentration as a result of a competition between diffusion and reaction of gas molecules which have entered from the surface of the sensing film [23]. The other specific feature of the plot is the short response and recovery times. The time taken by the sensor to achieve 90% of the total resistance change in the presence of NO_2 and N_2 was defined as the response and recovery time, respectively. The calculated response and recovery times for 47 ppm NO_2 gas at 450 °C was about 60–150 s. Fig. 12 illustrates the cyclic response of sensor at the

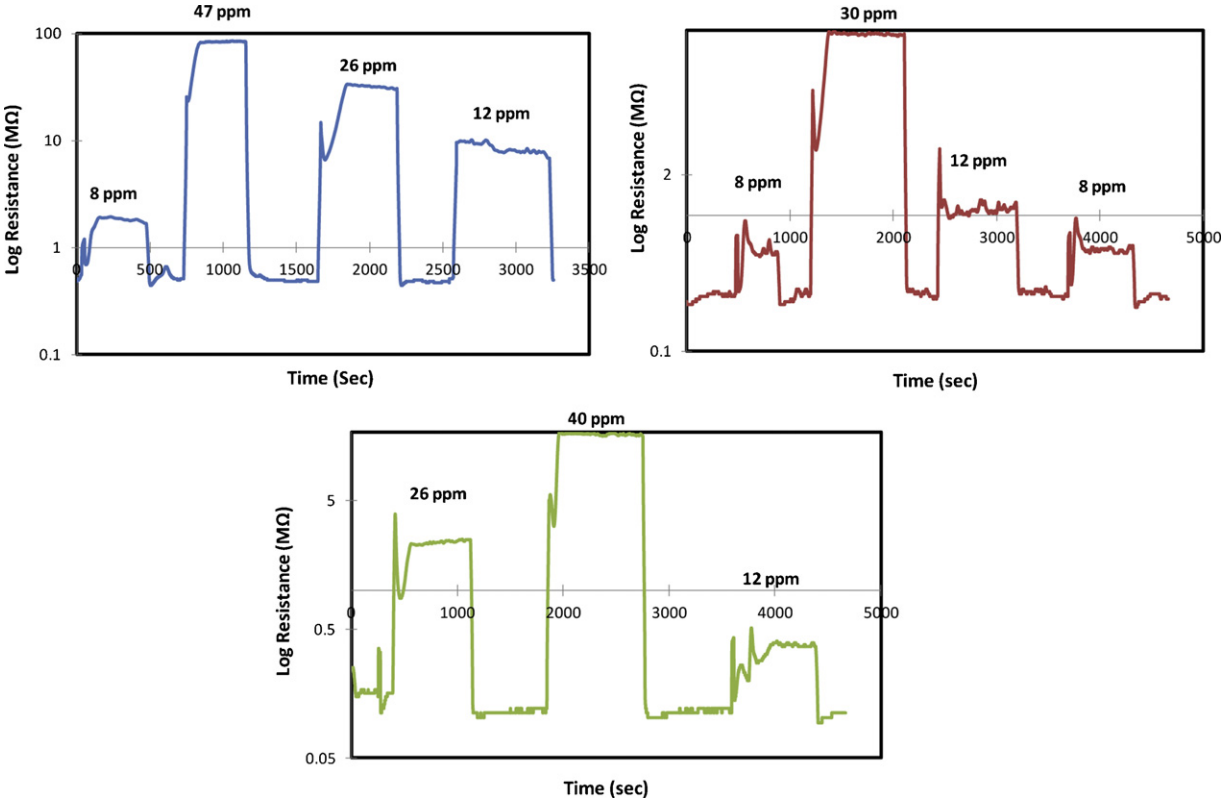

Fig. 11. Dynamic response of sensor exposed to NO_2 gas at the different temperatures.

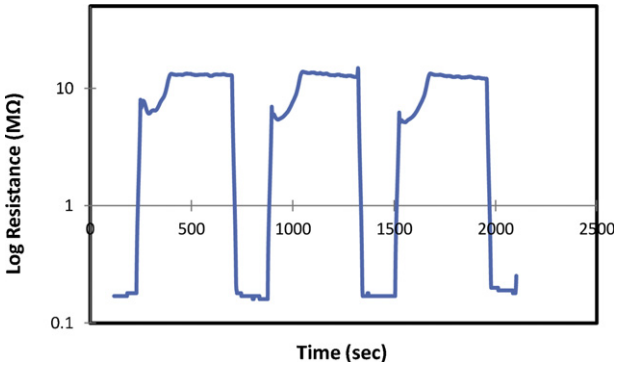

Fig. 12. Resistance changes versus time upon introduction and removal of 15 ppm NO_2 at temperature of 450 °C.

operating temperature with the highest response for 15 ppm NO_2 gas. It is clearly observed that the sensor has a repeatable and reliable behavior which is a good feature for gas sensing properties.

Originally, in the case of the sensors presented here, the suitable sensing properties is the result of the presence of high volume of sensing material exposed to the target gas due to the porous structure of the layer made by ACEPD method presented in Fig. 9.

4. Conclusion

The addition of Dolapix as dispersant to the TiO_2/acetone system resulted in an increase in the suspended particles' surface charge as well as the conductivity of the system. Also, the deposition behavior of TiO_2 nanoparticles under AC electric field at 1 Hz showed that by adding dispersant the deposition pattern was strongly changed. NO_2 gas sensor based on undoped TiO_2 nanoparticles was fabricated using AC electrophoretic deposition from suspensions containing dispersant. The sensing behavior of the fabricated sensor was studied in presence of NO_2 gas in the temperature range of 450–550 °C.

References

[1] E.K. Heidari, C. Zamani, E. Marzbanrad, B. Raissi, S. Nazarpour, WO_3-based NO_2 sensors fabricated through low frequency AC electrophoretic deposition, Sens. Actuators B: Chem. 146 (2010) 165–170.
[2] D.E. Williams, Semiconducting oxides as gas-sensitive resistors, Sens. Actuators B: Chem. 57 (1999) 1–16.
[3] B. Koo, J. Park, Y. Kim, S.-H. Choi, Y.-E. Sung, T. Hyeon, Simultaneous phase- and size-controlled synthesis of TiO_2 nanorods via non-hydrolytic sol gel reaction of syringe pump delivered precursors, J. Phys. Chem. B 110 (2006) 24318–24323.
[4] M.H. Seo, M. Yuasa, T. Kida, J.S. Huh, K. Shimanoe, Gas sensing characteristics and porosity control of nanostructured films composed of TiO_2 nanotubes, Sens. Actuators B: Chem. 137 (2009) 513–520.
[5] N. Barsan, D. Koziej, U. Weimar, Metal oxide-based gas sensor research: how to? Sens. Actuators B: Chem. 121 (2007) 18–35.
[6] A.R. Gardeshzadeh, B. Raissi, E. Marzbanrad, Electrophoretic deposition of SnO_2 nanoparticles using low frequency AC electric fields, Mater. Lett. 62 (2008) 1697–1699.
[7] R. Riahifar, B. Raissi, E. Marzbanrad, C. Zamani, Effect of parameters on deposition pattern of ceramic nanoparticles in non-uniform AC electric field, J. Mater. Sci.: Mater. Electron. 22 (2011) 40–46.
[8] R. Riahifar, E. Marzbanrad, B. Raissi, C. Zamani, M. Kazemzad, A. Aghaie, Sorting ZnO particles of different shapes with low frequency AC electric fields, Mater. Lett. 65 (2010) 632–635.

[9] B. Raissi, E. Marzbanrad, A.R. Gardeshzadeh, Particle size separation by alternating electrophoretic deposition, J. Eur. Ceram. Soc. 29 (2009) 3289–3291.
[10] S. Ghashghaie, E. Marzbanrad, B. Raissi Dehkordi, Low-frequency electrophoretic deposition of ZnO nanoparticles: effect of organic medium on deposition pattern, J. Am. Ceram. Soc., doi:10.1111/j.1551-2916.2011.04527.x.
[11] P. Sowti khiabani, E. Marzbanrad, C. Zamani, R. Riahifar, B. Raissi, Fabrication of In_2O_3 based NO_2 gas sensor through AC-electrophoretic deposition, Sens. Actuators B: Chem., manuscript number: SNB-D-11-01351R2, http://dx.doi.org/10.1016/j.snb. 2012.01.028, in press.
[12] S. Gaydardzhiev, P. Ay, Characterization of aqueous suspensions of fumed aluminium oxide in presence of two Dolapix dispersants, J. Mater. Sci. 41 (2006) 5257–5262.
[13] S. Prakash Rao, S.S. Tripathy, A.M. Raichur, Dispersion studies of sub-micron zirconia using Dolapix CE 64, Colloids Surf. A 02 (2007) 553–558.
[14] M.P. Albano, L.B. Garrido, Processing of concentrated aqueous silicon nitride slips by slip casting, J. Am. Ceram. Soc. 81 (1998) 837–844.
[15] S. Mei, J. Yang, J.M.F. Ferreira, Comparison of dispersants performance in slip casting of cordierite-based glass-ceramics, Ceram. Int. 29 (2003) 785–791.
[16] L. Besra, M. Liu, A review on fundamentals and applications of electrophoretic deposition (EPD), Progr. Mater. Sci. 52 (1) (2007) 1–61.
[17] J. Esmaeilzadeh, E. Marzbanrad, C. Zamani, B. Raissi, Fabrication of undoped-TiO_2 nanostructure-based NO_2 high temperature gas sensor using low frequency AC electrophoretic deposition method, Sens. Actuators B: Chem. 161 (2012) 401–405.
[18] R. Riahifar, E. Marzbanrad, B. Raissi, C. Zamani, Role of substrate potential on filling the gap between two planar parallel electrodes in electrophoretic deposition, Mater. Lett. 64 (2010) 559–561.
[19] K.B. Singh, M.S. Tirumkudulu, Cracking in drying colloidal films, PRL 98 (2007) 218302.
[20] H.-M. Lin, C.-H. Keng, C.-Y. Tung, Gas-sensing properties of nanocrystallin TiO_2, Nanostruct. Mater. 9 (1997) 747–750.
[21] M.R. Ana, G. Sakai, A. Cornet, K. Shimanoeb, J.R. Morantea, N. Yamazoe, Cr-doped TiO_2 gas sensor for exhaust NO_2 monitoring, Sens. Actuators B: Chem. 93 (2003) 509–518.
[22] M.C. Carotta, M. Ferroni, D. Gnani, V. Guidi, M. Merli, G. Martinelli, M.C. Casale, M. Notaro, Nanostructured pure and Nb-doped TiO_2 as thick film gas sensors for environmental monitoring, Sens. Actuators B: Chem. 58 (1999) 310–317.
[23] N. Matsunaga, G. Sakai, K. Shimanoe, N. Yamazoe, Diffusion equation-based study of thin film semiconductor gas sensor-response transient, Sens. Actuators B: Chem. 83 (2002) 216–221.